AD

AD-E402 905

Technical Report ARWEC-TR-99009

EFFECT OF CONFINEMENT ON THE MECHANIAL RESPONSE OF COMPOSITE PLASTIC BONDED EXPLOSIVES

Donald A. Wiegand

February 2000

US ARMY
TANK AUTOMOTIVE AND
ARMAMENTS COMMAND
ARMAMENT RDE CENTER

U.S. ARMY ARMAMENT RESEARCH, DEVELOPMENT AND ENGINEERING CENTER

Warheads, Energetics & Combat-support Armament Center

Picatinny Arsenal, New Jersey

The views, opinions, and/or findings contained in this report are those of the author(s) and should not be construed as an official Department of the Army position, policy, or decision, unless so designated by other documentation.

The citation in this report of the names of commercial firms or commercially available products or services does not constitute official endorsement by or approval of the U.S. Government.

Destroy this report when no longer needed by any method that will prevent disclosure of its contents or reconstruction of the document. Do not return to the originator.

REPORT DOCUMENTATION PAGE

Form Approved
OMB No. 0704-01-0188

PLEASE DO NOT RETURN YOUR FORM TO THE ABOVE ADDRESS.

1. REPORT DATE *(DD-MM-YYYY)*	2. REPORT TYPE	3. DATES COVERED *(From - To)*
February 2000		

4. TITLE AND SUBTITLE
EFFECT OF CONFINEMENT ON THE MECHANIAL RESPONSE OF COMPOSITE PLASTIC BONDED EXPLOSIVES

5a. CONTRACT NUMBER

5b. GRANT NUMBER

5c. PROGRAM ELEMENT NUMBER

6. AUTHORS
Donald A. Wiegand

5d. PROJECT NUMBER

5e. TASK NUMBER

5f. WORK UNIT NUMBER

7. PERFORMING ORGANIZATION NAME(S) AND ADDRESS(ES)
ARDEC, WECAC
Energetics and Warheads Division (AMSTA-AR-WEE)
Picatinny Arsenal, NJ 07806-5000

8. PERFORMING ORGANIZATION REPORT NUMBER

9. SPONSORING/MONITORING AGENCY NAME(S) AND ADDRESS(ES)
ARDEC, WECAC
Information Research Center (AMSTA-AR-WEL-T)
Picatinny Arsenal, NJ 07806-5000

10. SPONSOR/MONITOR'S ACRONYM(S)
TACOM/ARDEC

11. SPONSOR/MONITOR'S REPORT NUMBER(S)
ARWEC-TR-99009

12. DISTRIBUTION/AVAILABILITY STATEMENT
Approved for public release; distribution is unlimited.

13. SUPPLEMENTARY NOTES

14. ABSTRACT

The mechanical properties of composite explosives are being studied as a function of mechanical confinement and three techniques for confinement were used. These are (a) a constant confining pressure obtained by oil immersion, (b) radial confinement of a cylindrical sample by a thick walled steel cylinder that surrounds the sample (negligible radial strain), and (c) radial confinement of thin wafers by the platen-sample friction. While many energetic materials fail by crack growth when unconfined (significant surface area free of stress), with all of these forms of confinement, they appear to fail by yield and plastic flow. For crystalline explosives (e.g., TNT and Composition B), the yield strength and the modulus are independent of confining pressure so that useful results can be easily obtained by use of the steel cylinder technique. However, for materials containing polymer binders, such as plastic bonded explosives, a constant confining pressure is used because these properties are found to significantly increase with this pressure. These results indicate the very significant role of the polymer binders in determining the mechanical properties of these energetic materials.

15. SUBJECT TERMS

16. SECURITY CLASSIFICATION OF:			17. LIMITATION OF ABSTRACT	18. NUMBER OF PAGES	19a. NAME OF RESPONSIBLE PERSON
a. REPORT	b. ABSTRACT	c. THIS PAGE			19B. TELEPHONE NUMBER *(Include area code)*
Unclassified	Unclassified	Unclassified	SAR	27	

ACKNOWLEDGMENT

The author is indebted to D. Idar and B. Asay for providing the samples of PBS 9501.

CONTENTS

FIGURES

INTRODUCTION

Energetic materials are often used under conditions of mechanical confinement; e.g., explosives by the steel casings and propellants by high pressures during burning. When modeling, the response of energetic materials to planned and unplanned mechanical stimuli, it is necessary to know the mechanical failure modes and other mechanical properties as a function of confinement. Previously reported studies indicate a change with confinement in failure modes, but not elastic properties for compression of polycrystalline explosives; i.e., TNT (trinitrotoluene) and Composition B, a composite of TNT and RDX (cyclotrimethylene trinitramine) (refs. 1 and 2). In addition, the yield strength observed with confinement is independent of confining pressure (ref. 2). The sample loading conditions for this work is shown in figure 1 and results for Composition B are given in figure 2. While studies of composite plastic bonded explosives also indicate a change in compressive failure mode with confinement, use of the same steel cylinder technique as used for TNT and Composition B indicates that the results cannot be interpreted in terms of properties independent of confining pressure (ref. 3). The exploratory work reported here was undertaken to investigate the confining pressure dependence of failure and other mechanical properties of plastic bonded explosives.

A cell designed to contain pressures up to at least 138 MPa was used to study the compressive mechanical properties as a function of confining pressure (ref. 4). Hydraulic oil was used as the confining medium and the sample in the form of a right circular cylinder was protected from the oil by use of a tight fitting tubular gun rubber shroud. A sketch of the sample shroud and sensors is given in figure 3. The ends of the sample were against steel platens and O-ring seals were used to prevent oil from reaching the sample. The samples were compressed along the cylindrical axis and two linear voltage differential transformers (LVDTs) were mounted to measure axial strains. They were spaced 180 deg apart around the circumference of the sample and the sample axial strain was taken as the average of the strains obtained from the two LVDTs. Two additional LVDTs were mounted to measure radial strains. They were placed at the sample axial mid-position and were also 180 deg apart around the sample circumference. The confining pressure is taken here as the cell hydrostatic pressure before the start of the axial compression. Measurements at atmospheric pressure were made in air.

Axial stress versus axial strain data in uniaxial compression was obtained using the above cell and an MTS servo-hydraulic system operated at a constant strain rate of 0.001/sec (refs. 1 and 5). The samples were right circular cylinders and were 3.81 cm (1.50 in.) in length and 1.90 cm (0.75 in.) in diameter. The end faces of all samples were coated with a lubricant (e.g., graphite) to minimize frictional effects between the sample and the loading platens. The measurements reported here were made at 25°C and samples were conditioned at temperature for at least 2 hrs before measurement. The dimensions at 0.1 MPa (atmospheric pressure) were used to obtain engineering stress and engineering strain.

Most of the samples are a composite (PBS 9501) containing 94% sugar (sucrose), and a binder composed of 3% Estane and 3% BDNPF/A (Bis(2,2-Dinitropropyl) Acetal/Formal). This composite was developed as an inert mechanical simulant for a plastic bonded explosive (PBX 9501) composed of 95% HMX (cyclotetramethylene tetranitramine), 2.5% Estane, and 2.5% BDNPF/A (ref. 6). The unconfined compressive mechanical properties of PBS 9501 are very similar

to those PBX 9501 (ref. 6). A few results are also given for PBX 9501 and for another composite, PAX 2A, made up of 85% HMX, 9% BDNPF/A, and 6% cellulose acetate butyrate. Samples of the composites were prepared by pressing into large billets and machining to size, and precautions were taken to insure that the cylinder end faces were adequately flat and parallel (refs. 6 through 8). The densities of all samples were in a narrow range close to the maximum theoretical (zero porosity) density.

RESULTS

In figure 4, the compressive axial stress-strain response of PBS 9501 is given for two confining pressures, 0.1 MPa (atmospheric pressure) and 34 MPa (5,000 psi). The former is generally considered as unconfined. There are several significant differences between the two curves in figure 4. These include (a) a change from strain softening after the maximum at 0.1 MPa to work hardening at 34 MPa; (b) an increase in the yield strength, σ_y; (c) an increase in the initial slope and so Young's modulus, E; and (d) a decrease in the strain at yield, all with increasing confining pressure, p. Although Young's modulus is defined as the initial slope at atmospheric pressure, the same terminology and symbol E is used here at higher confining pressures.

In one case, the yield strength, taken at the point at which the initial part of the stress-strain curve deviates from linearity (fig. 4), is extremely low (see below). To help characterize the data, a flow stress is taken as the stress at the intersection of a straight line fitted to the work hardening part of the stress-strain curve with the straight line fitted to the initial Young's modulus portion of the curve. This is indicated in figure 4 for the data at 34 MPa. The flow stress, the yield strength, Young's modulus, and the work hardening coefficient [slope of the work hardening portion of the curve (fig. 4)] are given in figures 5 through 8, respectively.

As shown in figure 2, the results for samples compressed axially while radically confined in a thick walled steel cylinder are similar in part to the confined case of figure 4 (ref. 2). However, in the plastic flow region of the confined curve of figure 2, the slope is determined primarily by the bulk modulus. This is not the case for the confined curve of figure 4.

The yield strength given in figure 6 for the sample compressed at 138 MPa lies considerably below the extrapolation of the straight line fitted to the other thee points of this figure. This sample was hydrostatically cycled from atmospheric pressure to 138 MPa to atmospheric pressure and again to 138 MPa before axial compression at the latter pressure. In addition, during the first cycle of confining pressure increase and decrease, this sample may have received some axial loading. Therefore, damage that may have been induced either by the hydrostatic pressure cycling or by the axial loading during the first cycle may account for the apparently low yield strength observed for this sample. All other samples were compressed hydrostatically to the indicated pressure and then axially loaded without additional hydrostatic cycling or loading. However, the results given in figures 5 and 7 indicate that the flow stress and the modulus are apparently not affected by the hydrostatic pressure cycling or possible axial loading during the first cycle of pressure cycling. Although there is more scatter in the results of figure 8, the data suggest that the work hardening coefficient is also not strongly influenced by this first cycle of pressure cycling. Additional measurements are necessary to resolve this matter.

Results qualitatively similar to those of figure 4 have been obtained for several other composites including PBX 9404, PBX 9501, PBX 9502, PAX 2A, and Composition B using another type of confinement (refs. 8 and 9). Uniaxial compression of cylindrical samples with length (L) to diameter (D) ratios (L/D) of approximately 0.1 and 1 are given in figure 9 for PAX 2A. The results of figure 9 for the smaller value of L/D are similar to the data of figure 4 at 34 MPa while the results for the larger value of L/D are of course similar to the data at 0.1 MPa of figure 4. The confinement in this case is due to the frictional forces between the sample ends and the compression platens. Calculations indicate that this confinement influences the strains only at short distances from the sample ends (ref. 10). Thus, for the larger value of L/D, this radial confinement has little or no measurable effect on the axial stress-strain curve, but for the smaller L/D, the effect is very pronounced as the results of figure 9 indicate. A yield strength can be obtained from the upper curve of figure 9 in the same manner as it was obtained from the upper curve of figure 4. From measurements of thin wafers of PAX 2A as a function of temperature and strain rate, a qualitative measure of the yield strength as a function of these parameters has been obtained (ref. 9). The initial slope of the upper curve of figure 9 (L/D = 0.1) is not meaningful because of instrumental effects.

The strain softening at 0.1 MPa (lower curves of figures 2, 4, and 9) has been attributed to crack growth processes (refs. 9 and 11). Therefore, the results of figures 2, 4, and 9 indicate that this crack growth is either strongly inhibited or absent for the confined conditions of these figures. The photograph of figure 10 shows pictorial evidence to support this conclusion. The sample compressed at 0.1 MPa shows extensive cracking or tearing, while the samples compressed at 69 and 138 MPa show no evidence of external cracking.

The total axial strain was different for each sample of figure 10 and it is clear from the figure that the retained or permanent axial strain also differs for each sample. The sample compressed at 0.1 MPa has, in addition to extensive cracking and tearing, a large radial expansion at the bottom, but negligible radial expansion at the top. A gradient of radial strain is often observed for this type of sample, this amount of axial compression and this confining pressure (atmospheric). The permanent axial strain for this sample is –5.2%.

In contrast, the samples compressed at 34 (not shown), 69, and 138 MPa do not exhibit evidence of surface cracking or tearing and the radial strain is much more uniform along the sample length (fig. 10). The permanent axial and radial strains are –10.8% and 4.5% for the sample compressed at 138 MPa and –38.8% and 27.1% for the sample compressed at 69 MPa (fig. 10). The permanent radial strain is actually somewhat larger at the ends than along the rest of the sample for these two samples. This apparently occurs because of plastic flow of the sample along the sides of the steel compression platens. Before compression, the sample and platen diameters are equal. However, with axial compression, the sample diameter increases much more than the diameter of the steel platens. Therefore, regions of the sample near the circumference at each end of the sample are not in contact with the respective platen and so plastically flow along the cylindrical side surfaces of the platens. Because of this effect, the sample ends are recessed as shown in figure 11 and the permanent axial strains given were measured in the recessions. The permanent radial strains were measured in regions of uniform radial strain away from the sample ends.

In an effort to determine if the samples that were compressed while confined have significant internal cracking, the changes in volume and density were estimated for the sample compressed at 138 MPa. The fractional volume change ($\Delta V/V$) was estimated from the values given for the permanent axial strain ($(\Delta L/L)$, the permanent radial strain ($\Delta D/D$), and the relationship

$$\Delta V/V = \Delta L/L + 2\Delta D/D = -10.8 + 2 \times 4.5 = -1.8\% \quad (1)$$

where as noted, $\Delta L/L$ and ($\Delta D/D$ were measured away from the non-uniformly damaged sample ends. The non-uniformly damaged sample ends were then removed by cutting along planes perpendicular to the sample axis and the remaining sample was further cut in half by cutting along the sample axis. The density of one of the halves was determined by weighing in air and water and the density change due to confined compression was found to be

$$\Delta\rho/\rho = -1.0 \pm (0.5)\% \quad (2)$$

where ρ and $\Delta\rho$ are the density and the change in density, respectively. The rather large uncertainty in equation 2 is due to the difficulty of determining the sample weight in water because of the solubility of sugar, the main constituent of the composite in water. Both the volume and density changes as given in equations 1 and 2 are small compared to the permanent axial and radial strains and indicate that this sample has deformed primarily at constant volume and so without extensive internal cracking. The discrepancy between $\Delta V/V$ and $\Delta\rho/\rho$ is attributed to errors introduced because of the experimental difficulty of obtaining $\Delta V/V$ of a sample with non-uniformly damaged ends, and further, the experimental difficulty of determining the sample weight (and so density) in a liquid, water, in which the sample is soluble.

The results given in figures 5 through 8 indicate that the flow and yield stresses increase linearly with p, that E increases exponentially with p, and that the work hardening coefficient increases approximately in a linear fashion with p. The observed decrease of the strain at yield with increasing p is consistent with the fact that E increases faster with p than σ_y and indicates a difference from previously reported unconfined results as a function of temperature and strain rate. In the latter case, σ_y (σ_m) was found for several similar composites including PBX 9501 to be proportional to E and a failure strain (ε_m) to be constant as temperature and strain were varied (refs. 8 and 12). Increases in the yield or flow stresses and in the modulus with increasing confining pressure have been reported for polymers and polymer composites, including gun propellants (refs. 13 through 15). However, the increases per unit confining pressure increase for PBS 9501 are significantly greater than those reported in these references. The modulus increases by about a factor of 20 and the yield strength is estimated to increase by a factor of at least 10 with a confining pressure increase from 0.1 to 138 MPa. Thus, at 138 MPa, the estimated yield strength and the modulus of PBS 9501 are about 60% of the values of aluminum and 20% of the values of steel, the latter two at 0.1 MPa (ref. 16). Therefore, at the confining pressures used in this work, this composite has metal-like properties; i.e., it fails by yield and plastic flow and the yield strength and the modulus approach the values of metals. This behavior is to be contrasted with the sometimes brittle ceramic-like properties when unconfined.

As noted, measurements were also made of the radial strain at the sample mid-plane. From the slope of the radial strain versus axial strain curve, the value of Poisson's ratio is found to be about 0.34 at 0.1 MPa confining pressure. At higher confining pressures, this slope is reduced, but the smaller strains and attendant lower signal to noise ratios preclude giving meaningful values of Poisson's ratio at this time.

DISCUSSION

A discussion of the general nature of pressure dependence of the stress versus strain curve is followed by a discussion of the pressure dependence of the yield strength, the modulus, and the work hardening coefficient.

The yield strength is taken as the threshold stress for the initiation of the yield process and the flow stress is taken as the stress necessary for significant plastic flow. The data of figure 6 suggests that the onset of yield that is characterized by a deviation from linearity of the stress versus strain curve (fig. 4) is of the same nature at 0.1 MPa and at the higher confining pressure, but that the yield strength increases with pressure. However, the extrapolation of the flow stress versus pressure curve of figure 5 to 0.1 MPa indicates a flow stress at this pressure of about 30 MPa. Yet the maximum stress that is observed at 0.1 MPa is only about 8 MPa as shown in figure 4. These results suggest that after yield at 0.1 MPa, the crack growth processes that are responsible for the strain softening so weaken the sample that the stress necessary for significant plastic flow cannot be attained. After yield at the higher confining pressures, these crack growth processes are apparently so sufficiently inhibited by the confinement, that this weakening does not occur and the stress necessary for significant plastic flow is attained. Thus, the results indicate that at 0.1 MPa yield is followed primarily by crack growth processes while at the higher confining pressures yield is followed primarily by plastic flow and work hardening. The transition from yield and crack growth (strain softening) to yield, plastic flow, and work hardening is shown qualitatively as a function of L/D and so confinement in figure 12 for PBX 9501. As L/D is decreased, the effect of the confinement at the end surfaces is increased so that crack growth processes, and so the strain softening are reduced and the stress at any strain greater than the strain at the maximum stress is increased (ref. 9). This increase of stress allows increased plastic flow to take place. The initial slope of the upper curve of figure 12 (L/D = 0.08) is not meaningful because of instrumental effects. Similar results have been obtained for PBX 9404, PBX 9502, PAX 2A (fig. 9), and Composition B.

As pointed out, polymers exhibit the type of confining pressure dependence found here for the initial slope E and for the yield strength σ_y (ref. 15). Therefore, the results presented here support the conclusion made from the temperature and strain rate dependencies of these quantities; i.e., that these mechanical properties are strongly influenced by the polymer content of this and similar composites, even though the polymer content is in this case only 3.0% (ref. 9). Thus, the initial part of the stress-strain response, which is characterized by the E and σ_y, is strongly influenced by the polymer content of the composite.

The confining pressure dependence of the yield strength can be understood very simply in terms of the Coulomb yield criteria in which a frictional stress on the slip plane resists yield (ref. 17). This frictional stress is proportional to the total normal stress on the slip plane and so increases linearly with the applied confining pressure. The equation for the yield strength can then be written as

$$\sigma_y = b + c\,p \tag{3}$$

where σ_y is the applied axial stress at yield, p is the applied confining pressure, and b and c are constants.

A mark of this type of yield criteria is that the plane of maximum shear stress is not at 45 deg with respect to the applies compressive stress as is usually the case without friction, but at an angle whose deviation from 45 deg is dependent on the friction coefficient (ref. 17). Thus, evidence for or against this type of yield criterion can be obtained from the slip direction when it is known. The slip direction has not as yet been identified for this composite.

A linear increase of the yield strength with increasing confining pressure has also been attributed to a linear increase with confining pressure of the thermal activation energy for plastic strain (ref. 18). This activation energy must also decrease linearly with increasing applied axial stress. The jump frequency ν in the direction of the applied stress is then given by

$$\nu = \nu_o e^{-(U+\alpha p-\beta\sigma)/kT} \tag{4}$$

where ν_o is the vibrational frequency, U is the zero stress, zero pressure activation energy, p is the confining pressure, σ is the applied axial stress, T is the temperature, and α and β are activation volumes for the pressure and the stress, respectively (ref. 18). ν is assumed to be proportional to the plastic strain rate which at yield is approximately equal to the total strain rate. Then, from equation 4, the yield strength σ_y is given by

$$\sigma_y = \left[U + \alpha p + kT\ln\left(\dot{\varepsilon} / \varepsilon_o\right)\right]/ \beta \tag{5}$$

where $\dot{\varepsilon}$ is the strain rate and ε_o is a constant. Thus, this model predicts the temperature, strain rate, and confining pressure dependencies of the yield strength, and in particular, predicts the observed linear dependence of the yield strength on confining pressure at 25°C and a constant strain rate. Yet, analysis of limited published data as a function of temperature and strain rate at atmospheric pressure indicates that this material does not satisfy the predictions of this model (ref. 6). In addition, more extensive data for PBX 9501, also at atmospheric pressure, do not satisfy this model (ref. 9). However, the results also indicate that the mechanism of failure may not be the same at 0.1 MPa and at 34 MPa and above. Therefore, data as a function of temperature and strain rate at the higher confining pressures are necessary to conclusively determine the applicability of this approach.

The confining pressure dependence of the modulus might be due to two separate effects. The samples contain approximately 2.5% porosity that could be reduced by the confining pressure. Exponential dependencies of the modulus on porosity have been predicted and observed (refs. 19 and 20). Thus, the observed exponential dependence of the modulus on confining pressure follows if the porosity reduction varies linearly with confining pressure. This effect will saturate at sufficiently high confining pressures and additional measurements are necessary to determine the plausibility of this mechanism for modulus increase with increasing confining pressure. In addition, an increasing confining pressure forces the molecular chains of the polymer closer together, leading to increased stiffness because of an increased slope of the repulsive term in the energy versus intermolecular separation curve. The plausibility of this effect must also be assessed by additional work.

An extrapolation of the straight line fitted to the work hardening slope versus pressure data of figure 9 to 0.1 MPa indicates a very small slope or coefficient at this pressure. Thus, the work hardening is increased very significantly by the confining pressure. Because the processes of plastic flow are not established at this time, it is not possible to ascribe a mechanism to this work hardening. The plastic flow could take place primarily by dislocation interactions in the filler (sugar) of

the composite or more probably primarily by polymer processes in the binder. But whatever the mechanisms of plastic flow and work hardening, the efficiency of the work hardening process is very significantly increased by the confining pressure. Additional work is necessary to develop an understanding of these processes.

And finally, some of the reasons are now apparent for why the data obtained by compressing plastic bonded explosives in the thick walled steel cylinder (fig. 1) are not easily interpreted. The data of figures 5 through 8 indicate significant pressure dependencies of the yield strength, the flow stress, the modulus, and the work hardening slope. For the thick walled steel cylinder, the hydrostatic component of the stress taken as the average of the three principal stresses increases continuously from zero as the axial stress increases (fig. 2). Thus, the modulus and so the slope increases continuously until yield is attained. In addition, in the stress range above yield, the work hardening contribution to the slope will also increase with axial stress. Therefore, the linear regions of figure 2 for Composition B are curved for plastic bonded explosives, the yield point is not obvious and values for the modulus and yield strength not so clearly defined.

SUMMARY

These exploratory results indicate significant increases of the yield and flow stresses, the modulus and the work hardening coefficient with increasing confining pressure. In addition, crack growth processes that appear to account for the strain softening at a confining pressure of 0.1 MPa are not apparent at confining pressures of 34, 69, and 138 MPa. Instead, plastic flow and work hardening are observed at the later pressures. These results indicate that the dominant failure processes change from yield, crack generation, and growth at 0.1 MPa to yield and plastic flow at the higher confining pressures.

The rather strong confining pressure dependencies of the yield and flow stresses, the modulus, and the work hardening coefficient clearly account for the fact that compression of polymer containing composites in the thick walled confining cylinder, with the attendant strong change of the hydrostatic component of stress, did not give easily interpretable results. The results using the latter technique are most easily interpreted if the mechanical properties are independent of the hydrostatic component of stress.

The results also indicate that the mechanical properties of this polymer composite are more confining pressure dependent than some other polymers and polymer composites.

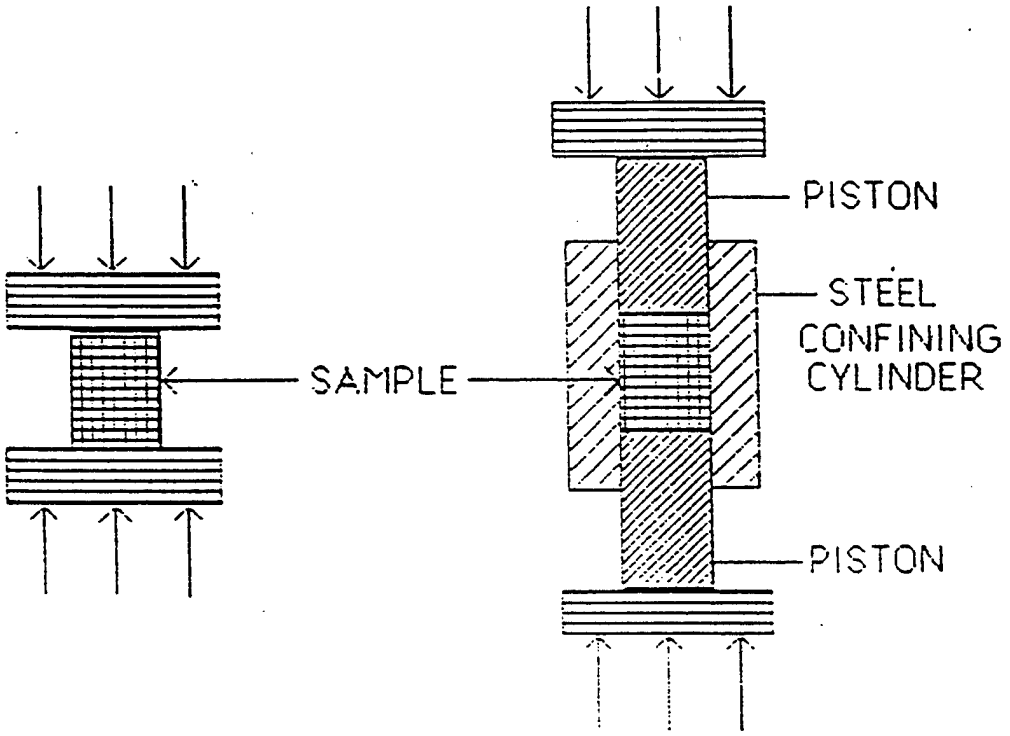

The samples are cylindrical and are compressed along the cylinder axis in each case

Figure 1
Sample and platen arrangements for (a) unconfined compression and
(b) confined compression in a thick walled steel cylinder

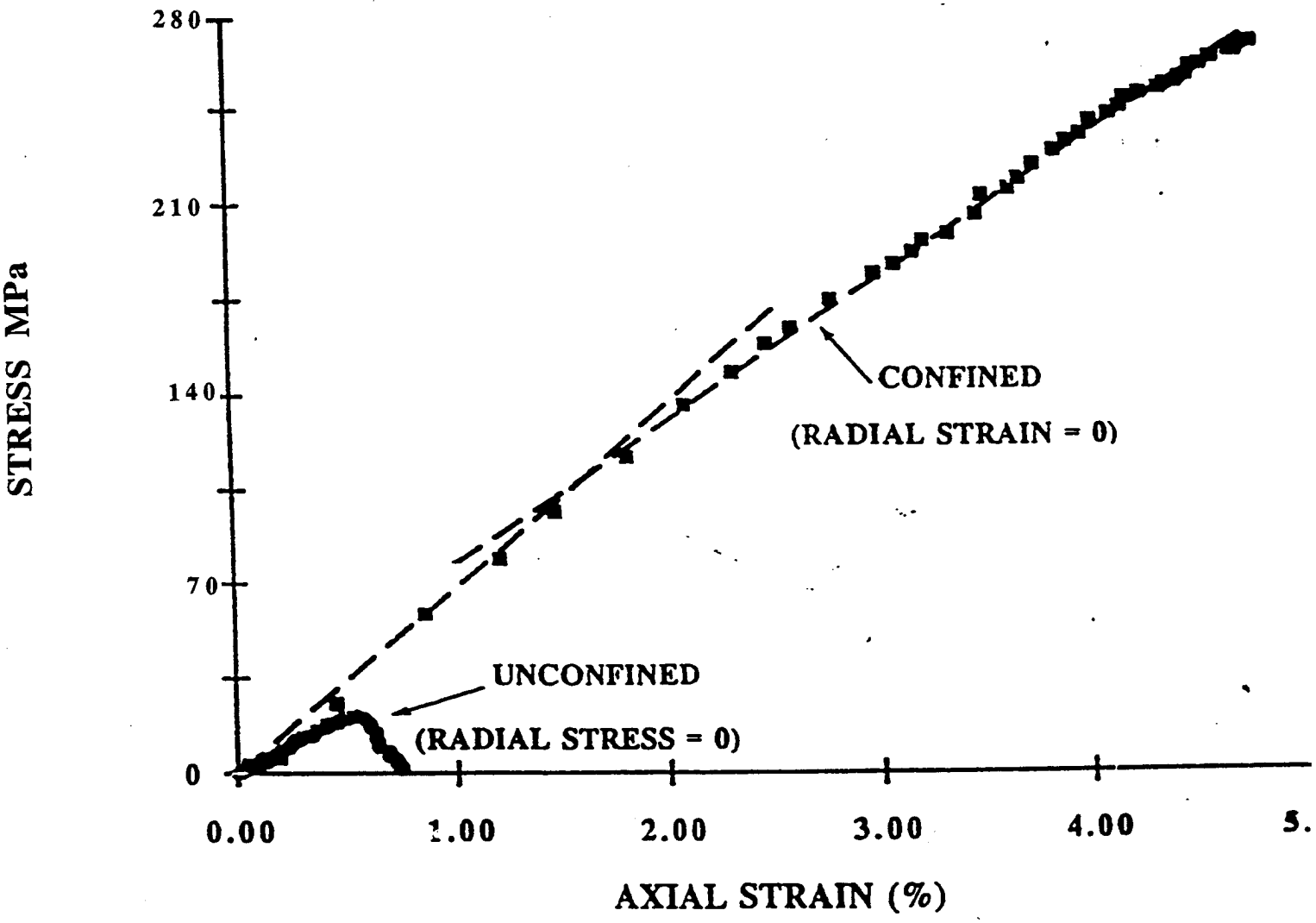

Figure 2
Axial stress versus axial strain for Composition B for the conditions of figure 1

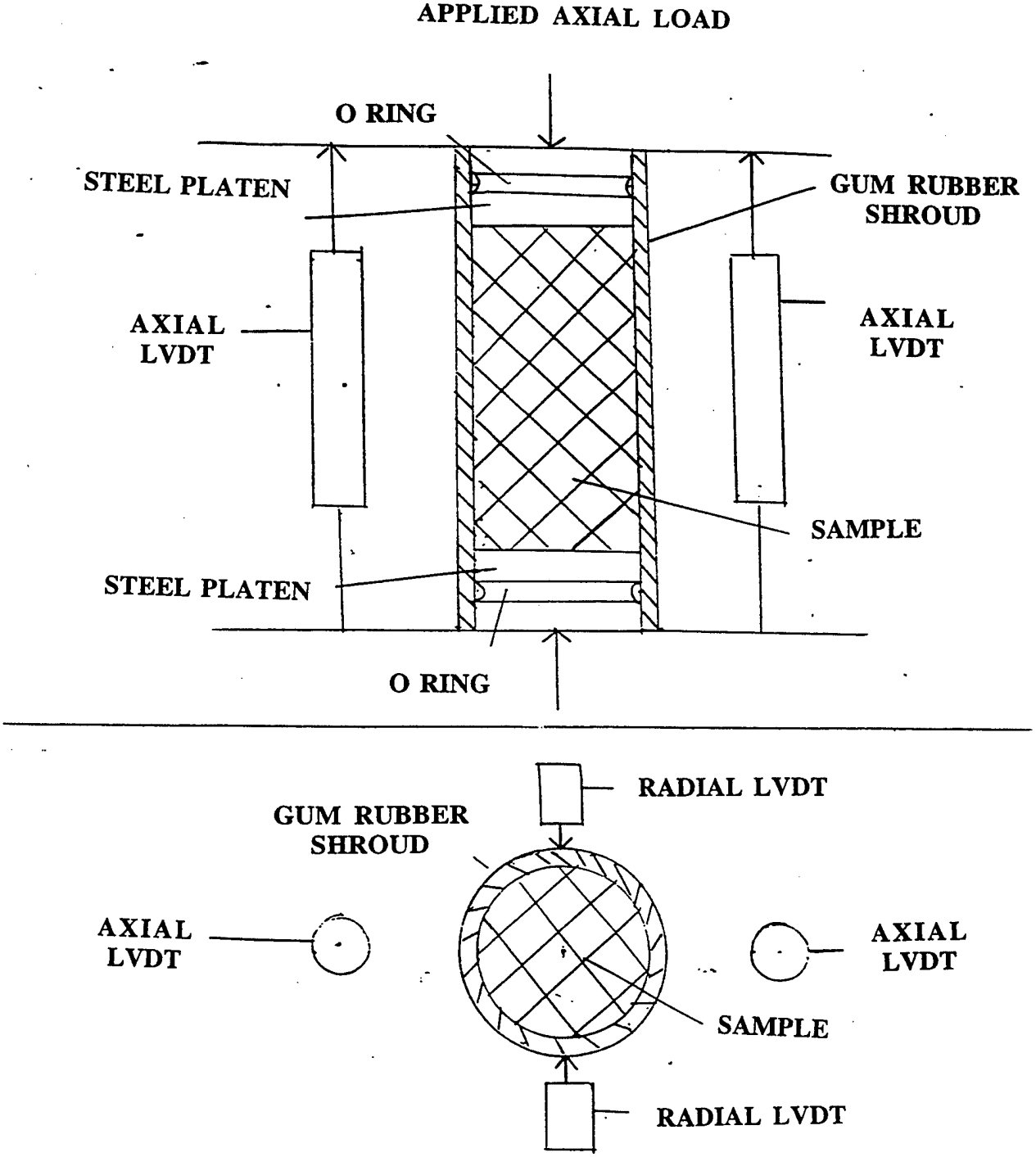

Figure 3
Side and end sketches of the sample, shroud and sensors for compression at constant pressure

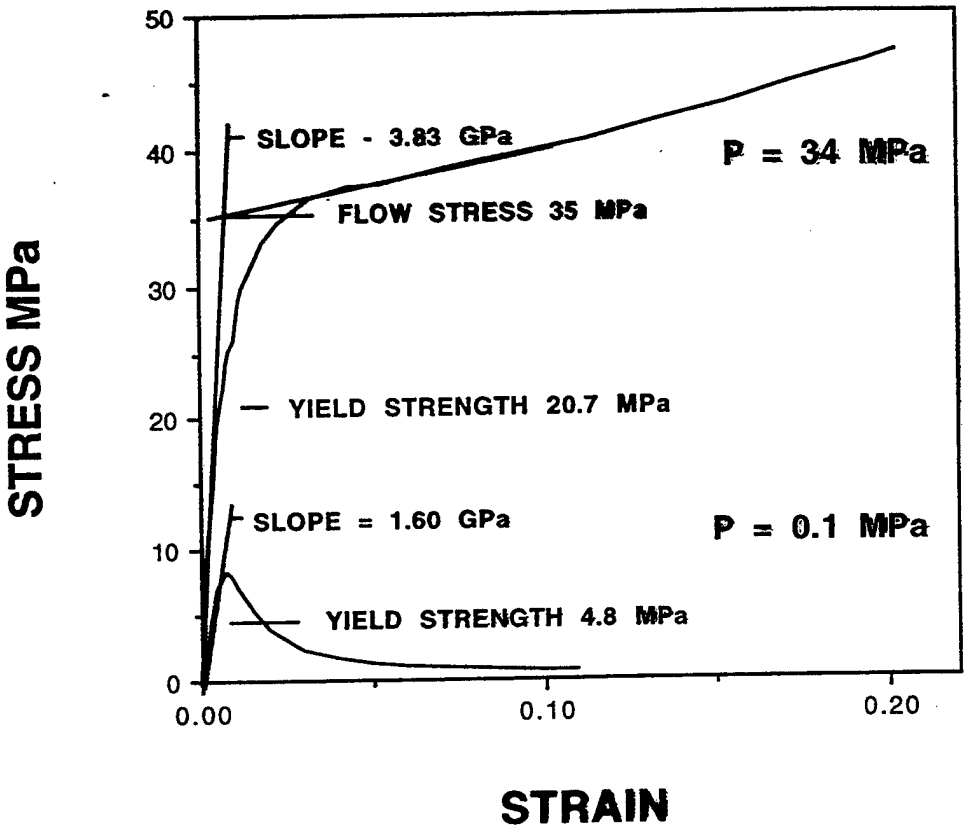

Figure 4
Axial stress versus axial strain for samples of PBS 9501 with confining pressures of 0.1 MPa (atmospheric) and 34 MPa

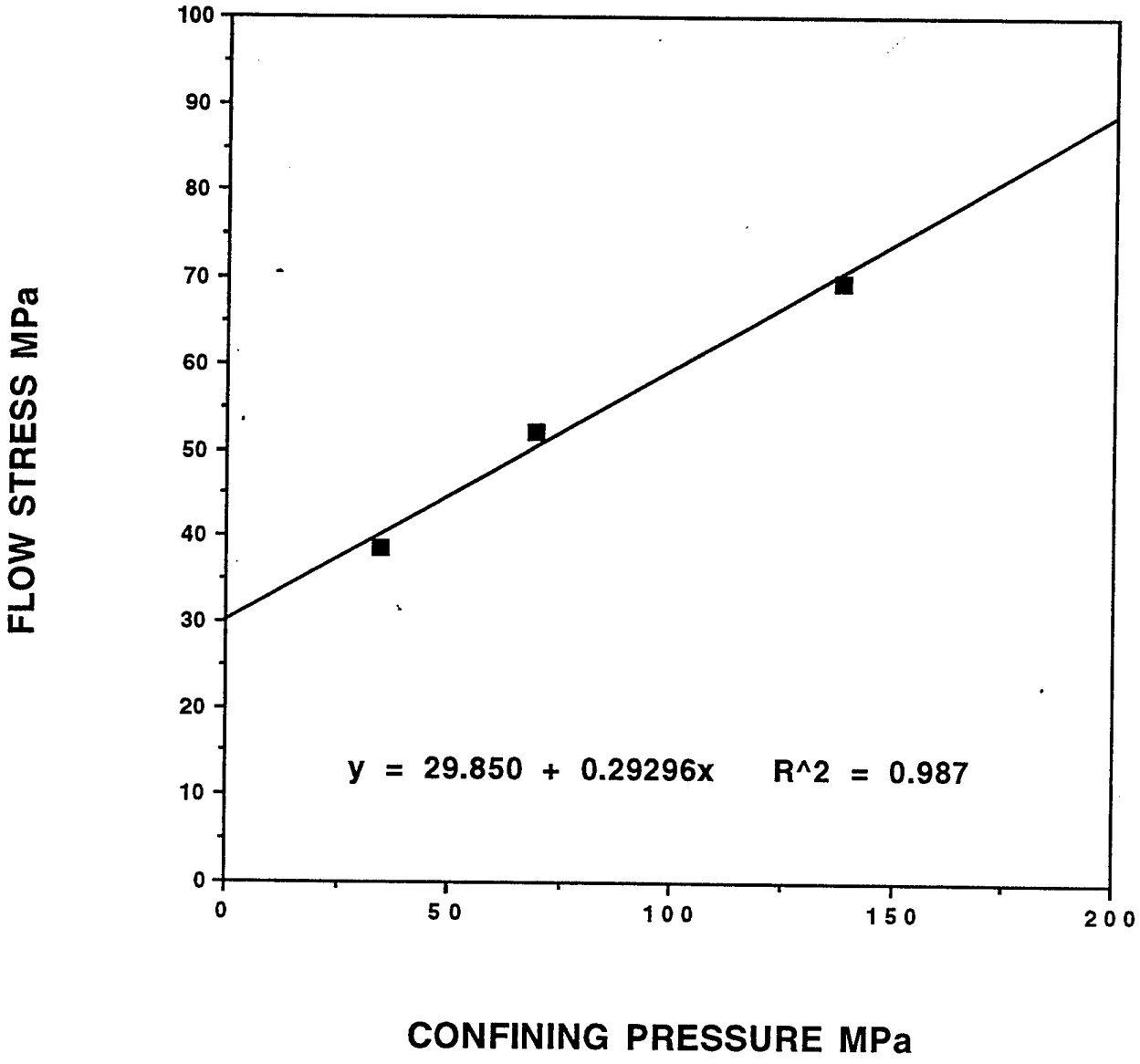

Figure 5
Flow stress versus confining pressure for PBS 9501

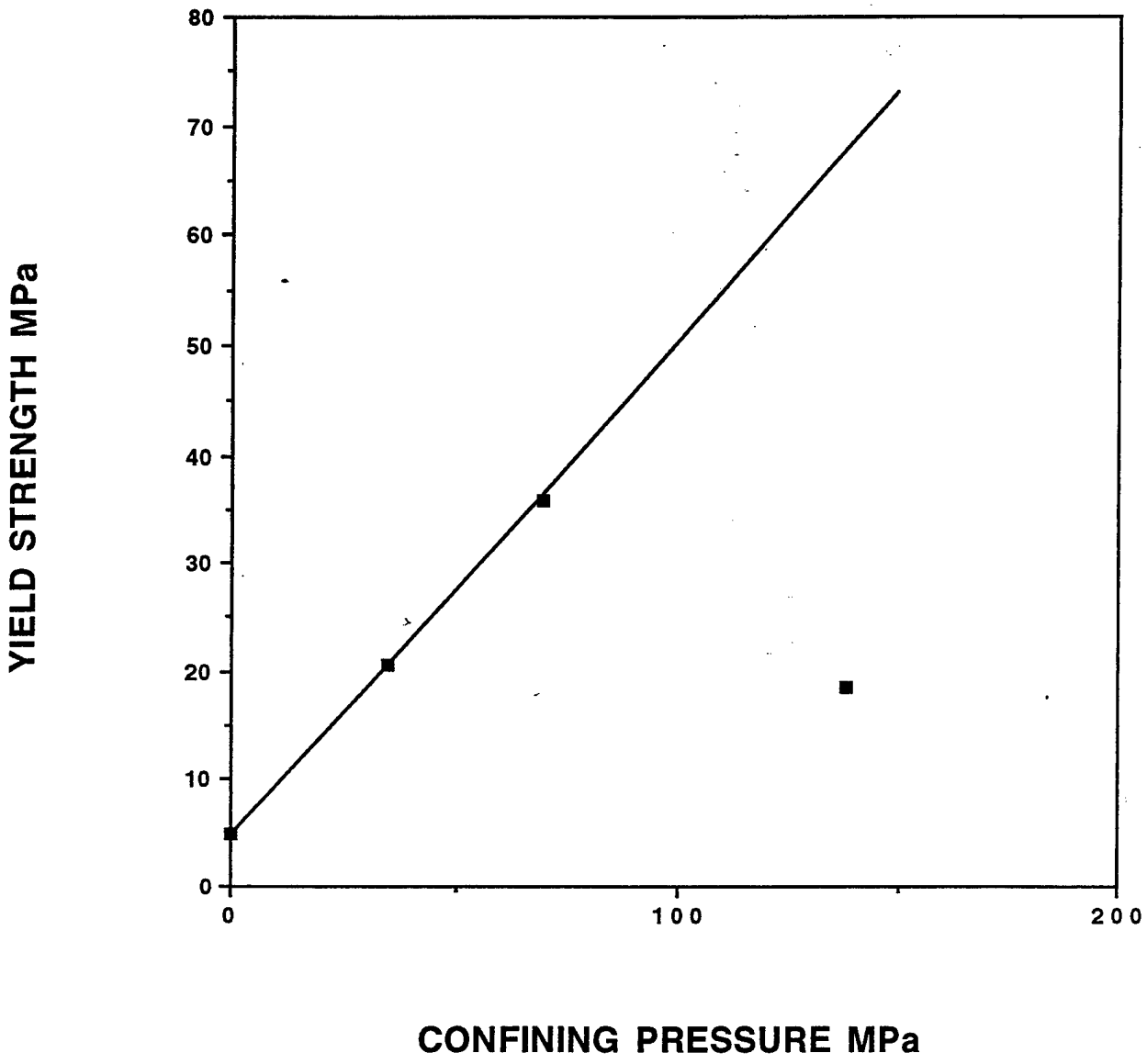

Figure 6
Yield stress versus confining pressure for PBS 9501

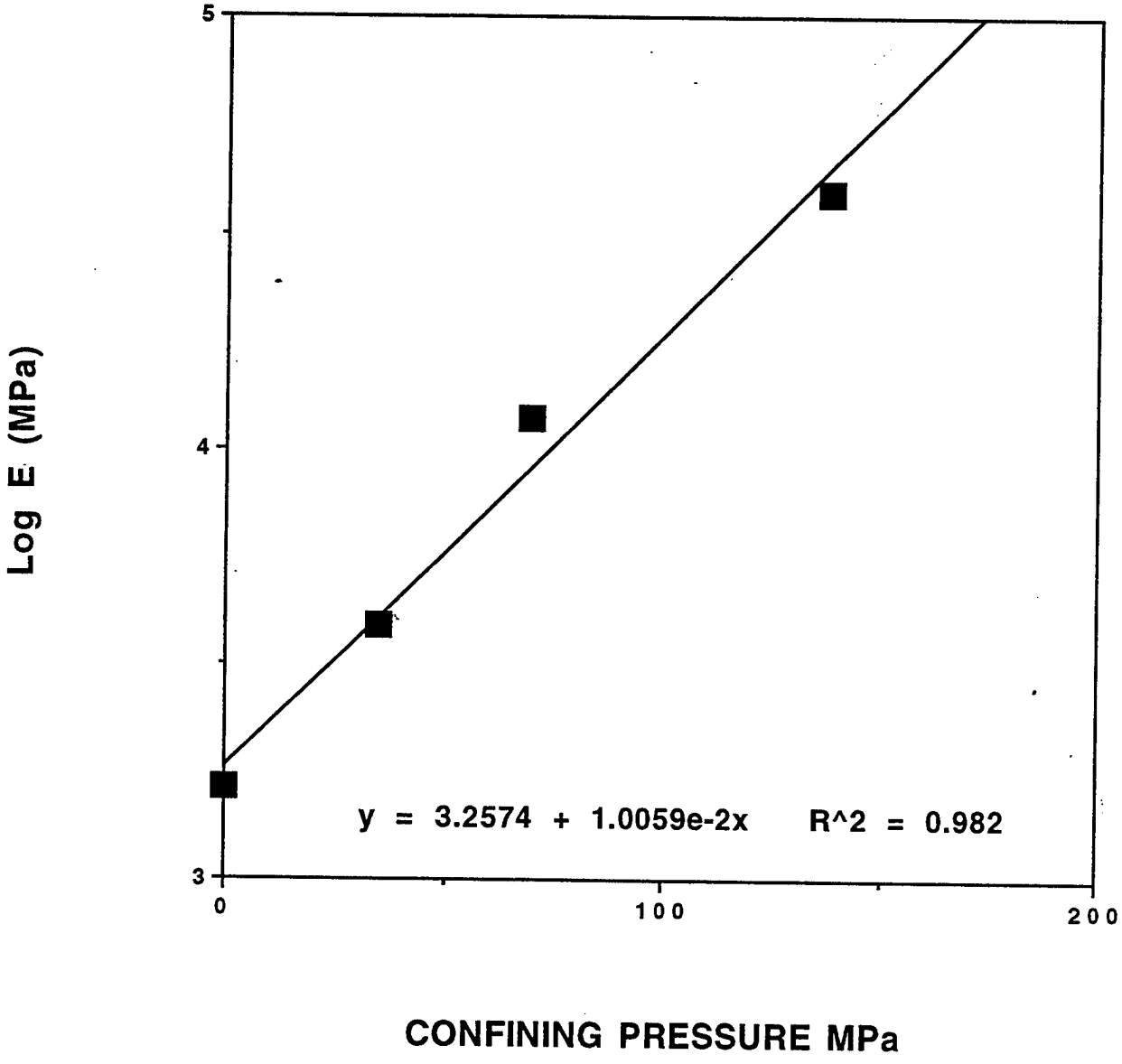

Figure 7
Log of Young's modulus versus confining pressure for PBS 9501

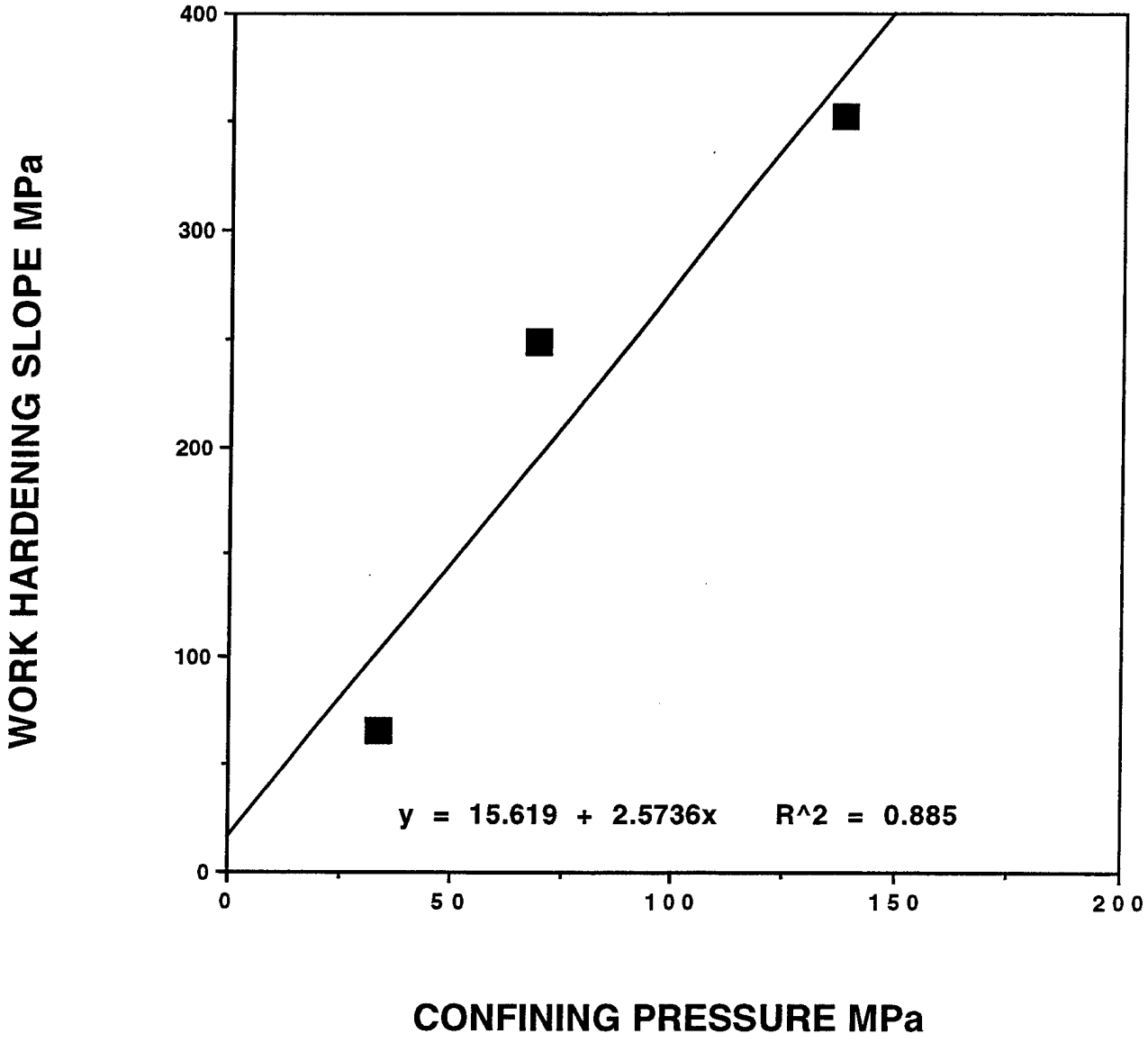

Figure 8
Work hardening slope versus confining pressure for PBS 9501

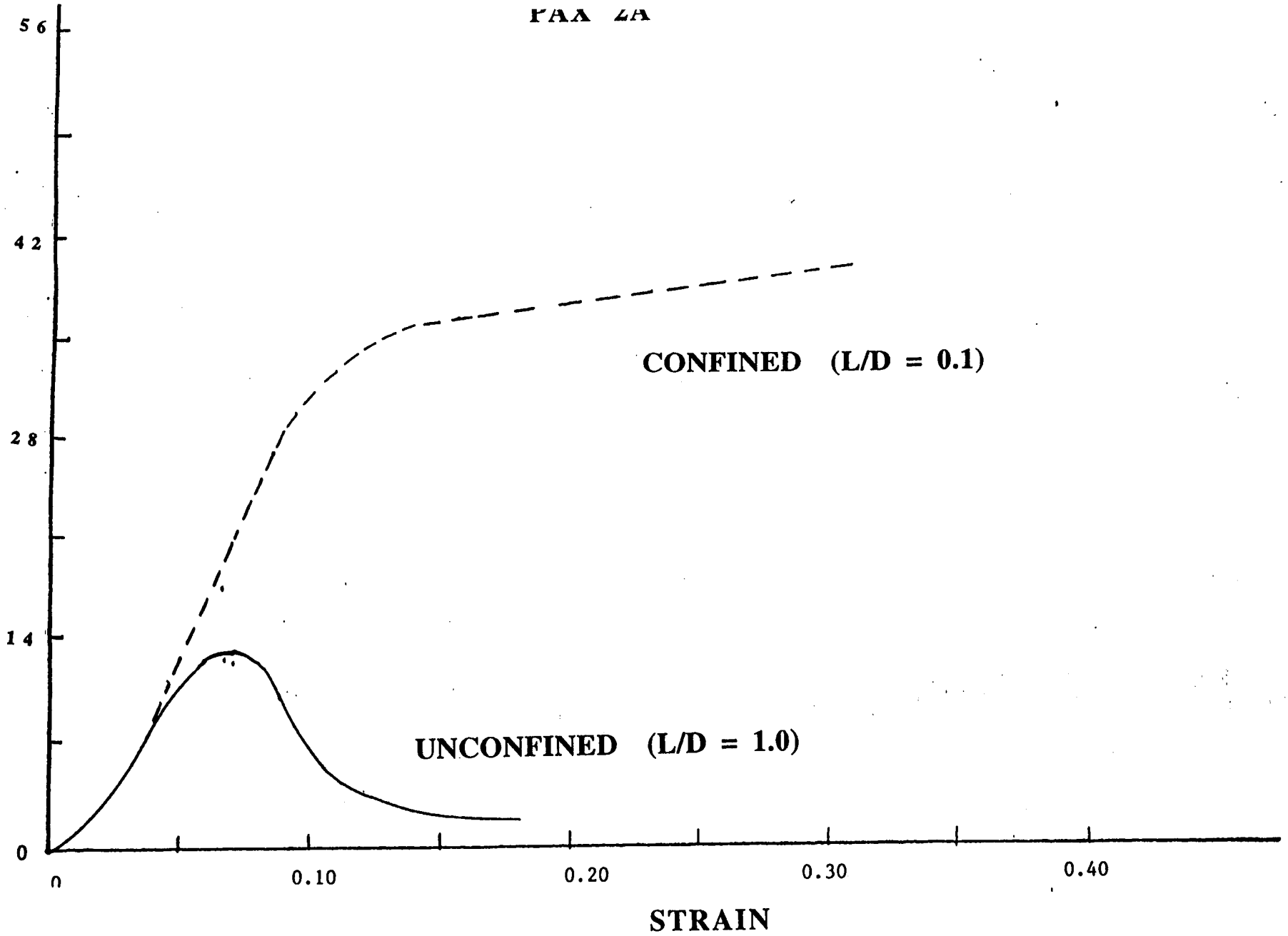

Figure 9
Axial stress versus axial strain for PAX 2A for cylindrical samples with length/diameter ratios of 1.0 and 0.1

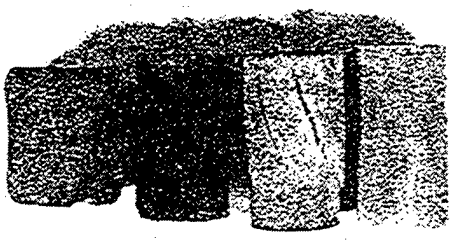

From left to right: undeformed sample and samples compressed axially with confining pressures of 0.1 MPa, 138 MPa, and 69 MPa. The maximum axial strain differs for each sample and the sample deformed at 138 MPa was graphite coated before deformation.

Figure 10
Photograph of an undeformed and deformed sample of PBS 9501

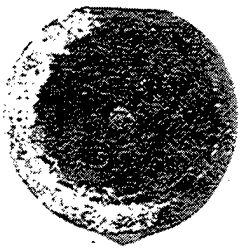

Figure 11
End view photograph of the sample of PBS 9501 that was deformed while confined at 69 MPa

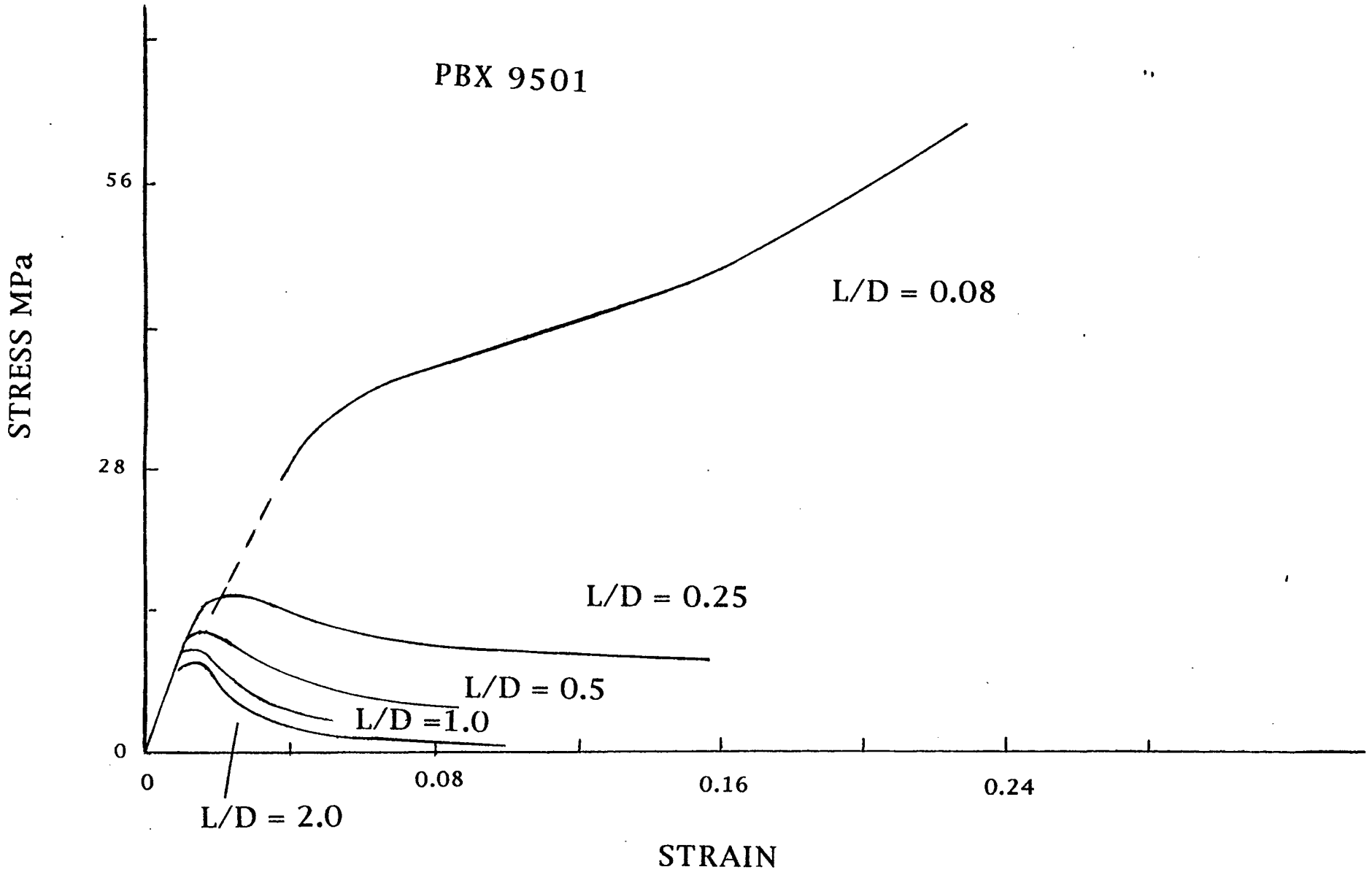

Figure 12
Axial stress versus axial strain for PBX 9501 for cylindrical samples with length/diameter ratios of 2.0, 1.0, 0.5, 0.25, and 0.08

REFERNCES

1. Weigand, D. A.; Pinto, J.; and Nicolaides, N., "The Mechanical Response of TNT and a Composite, Composition B, of TNT and RDX to Compressive Stress: I Uniaxial Stress and Fracture," J. Energetic Materials, 9, 19-80, 1991.

2. Pinto, J. and Wiegand, D. A., "The Mechanical Response of TNT and a Composite, Composition B, of TNT and RDX to Compressive Stress: II Triaxial Stress and Yield," J. Energetic Materials, 9, 205-263, 1991.

3. Mezgar, M.; Pinto, J.; and Wiegand, D. A., unpublished results.

4. Structural Behavior Engineering Laboratory, Phoenix, Arizona.

5. Pinto, J.; Nicolaides, S.; and Wiegand, D. A., "Dynamic and Quasi Static Mechanical Properties of Comp B and TNT," Technical Report ARAED-TR-85004, U.S. Army Armament Research, Development, and Engineering Center, Picatinny Arsenal, NJ 07805-5000, 1985.

6. Funk, D. J.; Laabs, G. W.; Peterson, P. D.; and Asay, B. W., "Measurements of the Stress-Strain Response of Energetic Materials as a Function of Strain Rate and Temperature: PBX 9501 and Mock 9501," in Shock Compression of Condensed Matter 1995, Woodbury, NY, pp 145-148, 1996.

7. Idar, D., private communication.

8. Wiegand, D. A., "Mechanical Failure of Composite Plastic Bonded Explosives and Other Energetic Materials," in Proceedings of the Eleventh International Detonation Symposium, 1988, in press.

9. Wiegand, D. A., unpublished results.

10. Rupel, A., unpublished calculations.

11. Dienes, J. K., "Strain-Softening via Scram," LA-UR-98-3620, 1998.

12. Wiegand, D. A., "Constant Critical Strain for Failure of Highly Filled Polymer Composites," in Proceedings of the 3rd International Conference on Deformation and Fracture of Composites, University of Surrey, Guildford, U.K., pp. 558-567, 1995.

13. Constantino, M. and Ornellas, D., "Initial Results for the Failure Strength of a LOVA Gun Propellant at High Pressures and Various Strain Rates," UCRL-92441, 1985.

14. Constantino, M. and Ornellas, D., "The High Pressure Failure Curve for JA2," UCRL-95555, 1987.

15. Ward, I. M. and Hardley, D. W., An Introduction to the Mechanical Properties of Solid Polymers, John Wiley & Sons, New York, NY, pp 234-236, 1993.

16. Handbook of Chemistry and Physics, 29th Edition, 1945.

17. Ward, I. M. and Hardley, D. W., An Introduction to the Mechanical Properties of Solid Polymers, John Wiley & Sons, New York, NY, pp 223-224 and 233, 1993.

18. Ward, I. M. and Hardley, D. W., An Introduction to the Mechanical Properties of Solid Polymers, John Wiley & Sons, New York, NY, pp 239-241, 1993.

19. Wang, J. C., J. Mat. Sci. 19, 801 and 809, 1984.

20. Wiegand, D. A. and Pinto, J., "Fracture and Yield Strengths of Composition B and TNT as a Function of Processing Conditions and Composition," Technical Report ARAED-TR-91002, U.S. Army Armament Research, Development and Engineering Center, Picatinny Arsenal, NJ, 1991.

DISTRIBUTION LIST

Commander
Armament Research, Development and Engineering Center
U.S. Army Tank-automotive and Armaments Command
ATTN: AMSTA-AR-WEL-T (2)
AMSTA-AR-GCL
AMSTA-AR-WEE-D, B. Fishburn
M. Mezgar
Y. Lanzerotti
D. Wiegand (10)
C. Hu
S. Nicolich
R. Surapaneni
AMSTA-AR-WEE-C, E. Baker
J. Orosz
AMSTA-AR-WEE, D. Downs
AMSTA-AR-QAR-R, L. Monole
E. Bixton
AMSTA-AR-QAR-V, F. Hihldebrant
AMSTA-AR-WEE-B, M. Paduano
AMSTA-AR-WEA, R. Rupel
S. Cytron
AMSTA-AR-WES, A. E. Siklosi
D. Fair
Picatinny Arsenal, NJ 07806-5000

Defense Technical Information Center (DTIC)
ATTN: Accessions Division (12)
8725 John J. Kingman Road, Ste 0944
Fort Belvoir, VA 22060-6218

Director
U.S. Army Materiel Systems Analysis Activity
ATTN: AMXSY-EI
392 Hopkins Road
Aberdeen Proving Ground, MD 21005-5071

Commander
Chemical/Biological Defense Agency
U.S. Army Armament, Munitions and Chemical Command
ATTN: AMSCB-CII, Library
Aberdeen Proving Ground, MD 21010-5423

Director
U.S. Army Edgewood Research, Development and Engineering Center
ATTN: SCBRD-RTB (Aerodynamics Technology Team)
Aberdeen Proving Ground, MD 21010-5423

Director
U.S. Army Research Laboratory
ATTN: AMSRL-OP-CI-B, Technical Library
AMXBR-BLT, R. Frey
AMXBR-BLC, J. Starkenberg
P. Baker
AMXBR-TBT, R. Lieb
G. Gazonas
Aberdeen Proving Ground, MD 21005-5066

Chief
Benet Weapons Laboratory, CCAC
Armament Research, Development and Engineering Center
U.S. Army Tank-automotive and Armaments Command
ATTN: AMSTA-AR-CCB-TL
AMSTA-AR-LCB-RA, J. Vasilakis
Watervliet, NY 12189-5000

Director
U.S. Army TRADOC Analysis Command-WSMR
ATTN: ATRC-WSS-R
White Sands Missile Range, NM 88002

Director
U.S. Army Materiel Systems Analysis Activity
ATTN: AMXSY-D
Aberdeen Proving Ground, MD 21005-5006

Commander
Naval Air Warfare Center Weapons Division
1 Administration Circle
ATTN: Code 473C1D, C. Dettling (2)
China Lake, CA 93555-6001

GIDEP Operations Center
P.O. Box 8000
Corona, CA 91718-8000

Office of the Secretary of Defense
OUSDA(A)
Director, Live Fire Testing
Washington, DC 20301-3110

Director
U.S. Army Aviation Research and Technology Activity
Ames Research Center
Moffett Field, CA 94035-1099

Commander
U.S. Army Missile Command
ATTN: AMSMI-RD-CS-R (DOC)
Redstone Arsenal, AL 35898-5010

HQDA (SARD-TR)
Washington, DC 20310-0001

Commander
U.S. Army Materiel Command
ATTN: AMCDRA-ST
5001 Eisenhower Avenue
Alexandria, VA 22333-0001

Commander
U.S. Army Laboratory Command
ATTN: AMSLC-DL
Adelphi, MD 20873-1145

Commandant
U.S. Army Infantry School
ATTN: ATSH-CD-CSO-OR
Fort Benning, GA 31905-5660

Commander
U.S. Army Aviation Systems Command
ATTN: AMSAV-DACL
4300 Goodfellow Blvd
St. Louis, MO 63120-1798

Commander
U.S. Research Office
ATTN: Chemistry Division
P.O. Box 12211
Research Triangle Park, NC 27709-2211

Commander
Naval Weapons Center
ATTN: L. Smith
A. Amster
R. Reed, Jr.
China Lake, CA 93555

Commander
Ballistic Missile Defense Advanced Technology Center
ATTN: D. Sayles
P.O. Box 1500
Huntsville, AL 35807

Air Force Armament Technology Laboratory
ATTN: AFATL/DOIL
AFATL/DLODL
Eglin Air Force Base, FL 32542-5438

Southwest Research Institute
ATTN: M. Cowperthwaite
6220 Culebra Road
Postal Drawer 28510
San Antonio, TX 78284

New Mexico Institute of Mining and Technology
ATTN: TERA, T. Joyner
Campus Station
Socorro, NM 87801

Director
Lawrence Livermore National Laboratory
ATTN: R. McGuire
K. Scribner
M. S. Costantino
J. Forbes
L-324
M. Finger
P. Harwood
S. Groves
P.O. Box 808
Livermore, CA 94550

Director
Los Alamos National Laboratory
ATTN: J960, J. Ramsay
MS B241, J. Dienes
MS P952, J. Dick
MS J567, D. J. Funk
MS C920, D. Idar
B. Asay
R. Gray
B. Blumenthal
P.O. Box 1663
Los Alamos, NM 87115

Southwest Research Institute
ATTN: H. J. Gryting
P.O. Box Drawer 28510
San Antonio, TX 78284

Honeywell, Inc.
ATTN: R. Tompkins
10400 Yellow Circle Drive
MN 38-330
Minnetonka, MN 55343

Commander
U.S. Army Armament Munition and Chemical Command
ATTN: AMSMC-ESM, W. D. Fortune
AMSMC-IRD, G. H. Cowan
Rock Island, IL 61299-6000

Director
Sandia National Laboratory
ATTN: MS 432, J. Aidun
MS 437, R. Thomas
MS 477, T. Chen
Box 5800
Albuqure, NM

John Hopkins University
Applied Physics Laboratory
Chemical Propulsion Information Agency
ATTN: John Hannum
Johns Hopkins Road
Laurel, MD 20707

Morton Thiokol, Inc.
Louisiana Division
ATTN: Lee C. Estabrook
P.O. Box 30058
Shreveport, LA 71130

Commander
Naval Weapons Station
ATTN: L. Rothstein
Code 50 – NEDED
Yorkstown, VA 23491